Soft Matter

PAPER

Universal spreading of water drops on complex surfaces

Cite this: *Soft Matter*, 2014, **10**, 2641

B. B. J. Stapelbroek,[a] H. P. Jansen,[b] E. S. Kooij,[b] J. H. Snoeijer[a] and A. Eddi[a]

Received 19th September 2013
Accepted 10th January 2014

DOI: 10.1039/c3sm52464g

www.rsc.org/softmatter

A drop of water spreads very rapidly just after it is gently deposited on a solid surface. Here we experimentally investigate how these early stages of spreading are influenced by different types of surface complexity. In particular, we consider micro-textured substrates, chemically striped substrates and soft substrates. For all these complex substrates, it is found that there always exists an inertial regime where the radius r of the wetted area grows as $r \sim t^{1/2}$. For perfectly wetting substrates, this regime extends over several decades in time, whereas we observe a deviation from a pure power-law for partially wetting substrates. Our experiments reveal that even the cross-over from the 1/2 power law to the final equilibrium radius displays a universal dynamics. This cross-over is governed only by the final contact angle, regardless of the details of the substrate.

1 Introduction

The spreading of a liquid drop on a substrate is relevant for many applications, ranging from agriculture to various industrial processes.[1–6] The final extent of drop spreading is governed by surface energies, provided that the surfaces can be considered homogeneous.[7,8] In a partial wetting situation, a liquid drop reaches a final shape defined by the equilibrium contact angle θ_{eq}, that is selected by Young's law. For perfectly wetting surfaces, by contrast, drops continue to spread over the surface. The radius of the wetted area grows as $r \sim t^{1/10}$ in the long-time limit, a result known as Tanner's law,[9] originating from a balance of capillary driving and viscous dissipation close to the contact line. This very slow spreading on perfectly wetting surfaces only stops when the drop height reaches a thickness that falls within the range of molecular interactions.

In contrast with this slow dynamics, the initial stages of drop spreading can be very fast[10–18] – here, the initial stage refers to the spreading starting at a radius $r = 0$ and followed on a small time scale after contact. This is due to a singularity, namely, at the instant of contact, the curvature of the interface is infinite, leading to a diverging Laplace pressure jump. This induces a rapid flow in the drop that replenishes the liquid neck, yielding a wetted area that grows in time. The initial stage of drop spreading is strongly reminiscent of the coalescence of two spherical liquid drops, which rapidly merge after contact is established.[17,19–24] The nature of the liquid plays an important role as the flow can be viscosity-dominated or inertia-dominated. For low-viscosity liquids such as water, there exists an inertial regime where $r \sim t^{1/2}$. This can be explained by the balance of the inertial pressure inside the drop, $\sim \rho(\mathrm{d}r/\mathrm{d}t)^2$, with the capillary pressure jump, $\sim \gamma R/r^2$, where ρ is the liquid density, γ its surface tension and R the initial drop radius. The spreading law is then given by

$$\frac{r}{R} = A\left[\frac{t}{t_c}\right]^{1/2}, \text{ with } t_c = \sqrt{\frac{\rho R^3}{\gamma}}, \quad (1)$$

where t_c is the inertio-capillary time (for water drops of $R = 0.5$ mm, $t_c \simeq 1.32$ ms). This law has been verified experimentally both for spherical drop coalescence[22,23] and for water drops spreading on a smooth and perfectly wetting glass substrate,[10,15] with $A = 1.2 \pm 0.1$ for both cases. The dynamics changes qualitatively for highly viscous drops, where a linear time-dependence (with logarithmic corrections) emerges both for coalescence[19,23,25] and spreading.[17] In addition, it was recently demonstrated for coalescence of freely suspended drops that both the viscous or inertial regimes are preceded by a phase where viscosity and inertia are equally important.[24] So far, such a visco-inertial regime has not been identified for spreading, and is expected to last for <100 nanoseconds for low-viscosity liquids such as water.

The role of the substrate during this initial stage of drop spreading is rather subtle.[11,13–15] Under perfectly wetting conditions, the substrate essentially acts as a mirror plane for the flow and does not affect the spreading law.[10] For water drops on partially wetting substrates, the dynamics is still dominated by inertia.[11] The spreading was found to be slower than the perfectly wetting case, eqn (1), and was interpreted as a change in power-law $r \sim t^{\beta}$, with β depending on the equilibrium contact angle.[11,18] Another view was provided by experiments and simulations that showed that the very early stages of drop

[a]*Physics of Fluids Group, MESA+ Institute for Nanotechnology, J. M. Burgers Centre for Fluid Dynamics, University of Twente, P. O. Box 217, 7500 AE Enschede, The Netherlands. E-mail: j.h.snoeijer@utwente.nl*

[b]*Physics of Interfaces and Nanomaterials, MESA+ Institute for Nanotechnology, University of Twente, P. O. Box 217, 7500 AE Enschede, The Netherlands*

spreading are independent of wettability, with $\beta = 1/2$, followed by a slowing down.[15] A detailed description for the slowing down on partial wetting surfaces is still lacking.

In this article, we will study how drop spreading is affected by three types of surface complexity: roughness, softness and chemical defects. It is well known that microtextured surfaces can have a pronounced influence on the equilibrium shape of a sessile drop. Using micro-pillars a drop can achieve a Wenzel state[26] but these substrates can be turned super-hydrophobic, in the so-called Cassie–Baxter[27–30] state. Such textures at a micro-scale also influence drop impact, and splashing is reduced as the air flow below the drop is modified[31,32]. Another substrate complexity can be introduced using chemical structures that change the wettability at a micro-scale.[33,34] Chemically patterned functionalization with alternating hydrophilic and hydrophobic stripes gives rise to anisotropic spreading. The final spreading of a liquid drop thus depends on the direction, resulting in elongated drops.[34,35] The chemical stripes can also be used to induce drop motion on the substrate.[36,37] A third kind of complexity can be introduced by making the substrate soft, and reducing the elastic modulus G' to a few tenths of kPa. On these substrates, the capillary forces near the contact line will pull on the substrate and induce a typical deformation of size $\sim\gamma/G'$, typically of the order of a few microns.[38–45] It has been found experimentally that the softness of the substrate slows down the wetting dynamics, an effect known as *viscous braking*, due to the visco-elasticity of the substrate.[46,47] This effect has been investigated experimentally for a spreading water drop, revealing that there exist several regimes depending on the liquid and substrate properties[14,18,48].

The goal of the paper is to reveal the early-stage spreading dynamics of water drops on these very different types of complex surfaces. In Section 2, we introduce the experimental set-up and the various substrates we use. Section 3 gathers the experimental results. We show that there always exists an initial inertial regime, that disappears earlier for more hydrophobic substrates. In Section 4, we analyse the nature of the cross-over observed for a partially wetting substrate. In Section 5, we discuss our results in terms of universal spreading behaviour. Surprisingly, we find that surface complexity does not play any role in the initial phase of drop spreading, and that the only relevant parameter to describe the underlying substrate effect is the advancing equilibrium contact angle θ_{adv}.

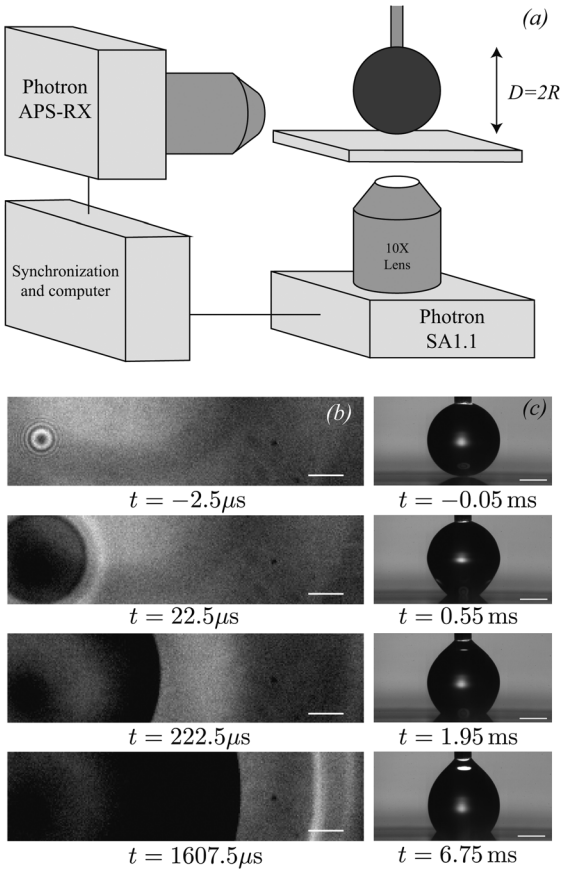

Fig. 1 (a) Sketch of the experimental set-up. (b) Series of snapshots of the bottom view for drop spreading on a smooth and partially wetting substrate. The white bar has a length of 50 μm. The fringes in the first recording of the bottom view are due to the interferences in the air layer separating the drop and the substrate. (c) Series of snapshots of the side view. The white bar has a length of 300 μm.

2 Experiments and methods

2.1 Experimental set-up

To investigate the initial dynamics of drop spreading on complex substrates, we use the set-up presented in Fig. 1(a). A water drop (Ultra-pure Milli-Q water, $\gamma = 0.072$ N m^{-1}, $\rho = 1000$ kg m^{-3}) is slowly grown at the tip of a needle until it touches the substrate. The distance between the needle and the substrate automatically sets the drop diameter $D = 1$ mm at the time of contact. Water is pumped at a low flow rate (10^{-3} mL min^{-1}), so that the approach velocity is lower than 20 μm s^{-1} and that the impact speed can be neglected.

To capture the initial stage of spreading, a transparent substrate is placed on a microscope, and the process is recorded with two synchronised high-speed cameras. A Photron SA1.1 camera coupled to an inverted microscope records a bottom view of the wetted area [Fig. 1(b)]. This allows for high speed recording with a frame rate up to 400 000 frames per s and a spatial resolution of 2 μm per pixel. Before contact between the drop and the substrate, one can observe fringes due to the thin air layer separating them. After contact, the wetted area appears as a circular dark area that grows with time. For all experimental data, we consider the contact time to be half-way in between the last frame where the fringes can be seen and the first frame where the dark area appears. This ensures a minimal error on the contact time determination. An APX-RS camera coupled to a long-range microscope records the side view [Fig. 1(c)]. It records the later times of spreading, with a frame rate of 10 000 frames per s, and a spatial resolution of 3.5 μm per pixel. The radius r of the wetted area is determined from the images using custom Matlab scripts. The bottom view is used to record the early dynamics of drop spreading, and is crucial for getting accurate measurements for $r < 100$ μm. Combining the two

views, we can determine the spreading dynamics over more than 3 decades in time and 2 decades in space.[15,17]

2.2 Complex substrates

In order to investigate the influence of the surface complexity on the spreading of a droplet, we vary the surface roughness, apply chemical heterogeneities on a microscale, and introduce substrate deformability by reducing its elastic modulus.

Microtextured substrates. We use glass substrates covered with a square array of cylindrical micro-pillars fabricated with standard photolithography and etching techniques [Fig. 2(a)]. Their height is kept constant at $H = 5$ μm, the diameter W of the pillars varies from 10 to 20 μm and their spacing S from 5 to 40 μm. These structures are cleaned using piranha solution (H_2SO_4/H_2O_2) and thus have a high wettability with a contact angle $\theta_{adv} < 5°$. This guarantees that the drops enter the space between the pillars and achieve a Wenzel state.

Chemically striped substrates. The chemically striped substrates consist of glass with alternating hydrophobic (PFDTS) and hydrophilic stripes (SiO_2) on the surface [Fig. 2(b)]. Static contact angles of 1 μL droplets were measured on pristine PFDTS and SiO_2 surfaces using an OCA15 + goniometer (Dataphysics, Germany). The values amount to $\theta_{PFDTS} = 110°$ and θ_{SiO_2}=40°, respectively. Contact angles measured using the sessile drop method are typically close to the advancing angles on these surfaces; the profile of the droplets was fitted with a circle. These are created using self-assembling perfluorodecyltrichlorosilane (PFDTS, ABCR, Germany) monolayers.[34] The width of the hydrophobic stripes is kept constant and is $w_1 = 10$ μm, the width of the hydrophilic stripes w_2 varies between 2 μm and 30 μm. We define $\alpha = w_1/w_2$ to characterize each substrate. On these substrates, the final spreading achieved is different along the direction parallel to the stripes and the one perpendicular to them,[34,35] resulting in an elongated droplet.

Soft surfaces. We prepared substrates with a low elastic modulus by applying a thin layer of polydimethylsiloxane (PDMS) with a film casting knife on a glass slide. The thickness of the soft layer is varied between 13 μm and 215 μm. The elasticity of the PDMS is varied by using three different mass ratios 1 : 10, 1 : 30 and 1 : 50, between the cross-linker (curing agent) and the pre-polymer (base),[14,18,49] resulting in a shear elasticity of: $G' = 1.1$ Mpa, $G' = 41$ kPa and $G' = 32$ kPa, measured at 1 Hz with a shear rheometer (TA Instrument DHR-3). After curing for one hour at 100 °C, the samples are washed several times in tetrahydrofuran (THF, C_4H_8O) to dissolve the non-cross-linked polymer chains. These substrates are naturally hydrophobic ($\theta_{adv} > 115°$), but they can be turned perfectly wetting by plasma cleaning them for 1 minute.

For all partially wetting substrates, the advancing equilibrium contact angle θ_{adv} is determined from the side view images when the contact line is not moving anymore. The obtained values are summarised in Table 1. The measured values are not the equilibrium contact angle, but also account for substrate hysteresis.[14,18,42,47,50,51] That is why the soft PDMS substrates with the same surface chemistry (and thus the same equilibrium contact angle) present different values for θ_{adv}.

3 Results

3.1 Microtextured substrates

Combining the bottom and side views we first consider the evolution of the wetted area r as a function of time t for a perfectly wetting micro-pillar structure with $H = 5$ μm, $W = 10$ μm and $S = 5$ μm [Fig. 3(a)]. As shown in the inset of the figure, short times and small radii are obtained from the bottom view, whereas the later dynamics are measured from the side view images. Each experiment is repeated at least five times to ensure the reproducibility of the recorded phenomena. The measured radii are then averaged and the error bar is given by the standard deviation of each dataset. In order to reveal the initial dynamics these experimental results are plotted in dimensionless units r/R and t/t_c on a logarithmic scale [$t_c = \simeq 1.32$ ms is the inertio-capillarity time defined in eqn (1)]. We observe that the radius of the wetted area grows as $r/R \propto (t/t_c)^{1/2}$ (the best fit is obtained for an exponent 0.55), in good agreement with the theoretical prediction. The data also agree quantitatively with those for water drops spreading on a perfectly wetting smooth substrate.[10,11,15] Throughout the paper, the data from Winkels *et al.*[15] for spreading on perfectly

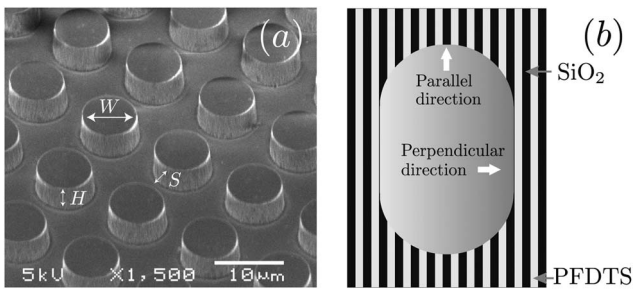

Fig. 2 (a) SEM image of the micro-pillar substrates. The parameters H, S and W are defined in the picture (b) alternating wetting and non-wetting stripes on the chemically coated structures. The width of the hydrophobic stripes is $w_1 = 10$ μm, the width w_2 of the hydrophilic stripes varies from 2 μm to 30 μm. The spreading directions parallel and perpendicular to the stripes are indicated by the arrows.

Table 1 Measured final advancing contact angles θ_{adv} for the micro-textured, chemically striped and soft substrates used in experiments

Micropillars	$\theta_{adv} < 5°$	
Chemical stripes	$\theta_{\perp}$	$\theta_{\parallel}$
$\alpha = 5$	107 ± 3°	97 ± 3°
$\alpha = 2$	95 ± 3°	81 ± 3°
$\alpha = 1$	91 ± 3°	69 ± 3°
$\alpha = 0.4$	83 ± 3°	63 ± 3°
$\alpha = 0.33$	77 ± 3°	45 ± 3°
Soft substrates		θ_{adv}
$G' = 32$ kPa		135 ± 5°
$G' = 1.1$ MPa		120 ± 5°

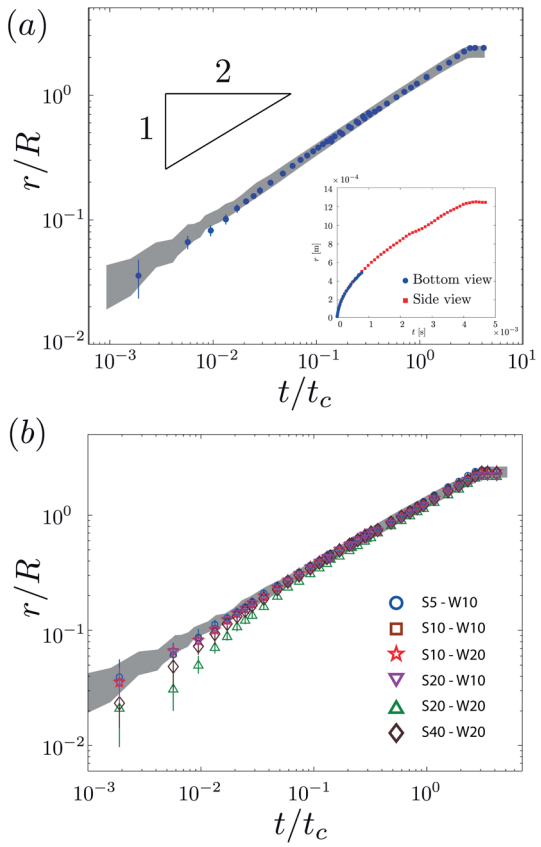

Fig. 3 (a) Dimensionless radius r/R as a function of dimensionless time t/t_c for a wetting micropillar structure ($S = 5$ μm, $W = 10$ μm, $H = 5$ μm) with a logarithmic scale. The inset is the data obtained for a single experiment in physical units with a linear scale. (b) Dimensionless radius r/R as a function of dimensionless time t/t_c for 6 different wetting micropillar structures.

wetting silica will be used as a reference case for all experiments; these data and their confidence interval are represented by the grey area in Fig. 3(a).

From this first experiment, we conclude that this pillar structure does not have any influence on the initial stages of drop spreading in a perfectly wetting situation. This unexpected result is further confirmed when comparing the spreading over surfaces with 6 different micro-pillar structures [Fig. 3(b)]. In all the cases we observe the same spreading behaviour agreeing with the reference case given by a smooth perfectly wetting glass substrate. The scatter in the initial part is due to the uncertainty in determining the contact time: as the droplet first touches the top of a pillar, the contact line spreads over it and then slides down to reach the bottom of the surface. This delay has almost no influence for a small pillar diameter W, but the uncertainty increases for a larger W. This scatter is completely smoothened out when the contact line has moved a few pillars away from the contact point. The wetted area then has a circular shape, confirming that the microstructure does not influence the spreading in this initial regime. The fact that the structure does not influence the geometry of the contact line maybe explained from the very small radius of curvature that drives the flow$\sim r^2/R$. During the initial stages, this is smaller than 10^{-6} m which is smaller than the typical size of the structure.

3.2 Chemically striped substrates

We now consider the spreading on chemically heterogeneous surfaces consisting of alternating hydrophilic and hydrophobic stripes. These surfaces have two different spreading directions, *i.e.* parallel and perpendicular to the stripes. Spreading in the direction perpendicular to the stripes is more difficult in comparison to the parallel direction due to relatively high energy barriers posed by the hydrophobic stripes over which the droplet has to advance. In the parallel direction such energy barriers do not exist; the extent of contact line motion is determined by the ratio of the widths of the hydrophobic and hydrophilic stripes, *i.e.* α. Due to the difference in the two directions a droplet deposited on such a surface typically adopts an elongated shape with two different final advancing contact angles $\theta_\perp$ and $\theta_{||}$. The elongation depends on α,[34] with lower α values resulting in more elongated droplets, due to more favourable advancing of the contact line in the parallel direction. We separately determine the spreading along these two axes. The results obtained for an $\alpha = w_1/w_2 = 0.4$ structure are presented in Fig. 4(a). We observe a smaller final radius of the drop along the perpendicular axis. The anisotropy of the surface is thus observed during the final stage of the spreading, resulting in an elongated final shape of the drop. However, during the initial stage, the spreading along both parallel and perpendicular directions follows the same dynamics. In addition, it agrees quantitatively with the spreading observed on a perfectly wetting and smooth glass substrate (gray area).

As can be seen in Fig. 4(b), the spreading is identical along the perpendicular direction whatever the value of α: the curves almost collapse on top of each other for the 5 different samples. This also implies that the final contact angle $\theta_\perp$ has only small variations with $\theta_{adv} = 90 \pm 15°$. This can be explained by the contact line pinning that occurs at the edge of the stripes. The details of this process are similar to zipping wetting observed on hydrophobic micro-textured substrates.[29,30] We also observe that the initial stage of spreading follows quantitatively the reference $r/R \propto (t/t_c)^{1/2}$ law for a smooth, perfectly wetting substrate.

In the parallel direction, the final radius increases with decreasing α [Fig. 4(c)]. This is expected as the surface is more hydrophilic for smaller α, where $\theta_{||}$ is given by the Cassie–Baxter equation.[27,35] For decreasing values of α, the hydrophilic stripes become wider and $\theta_{||}$ decreases from $\theta_{||} = 97°$ to $\theta_{||} = 45°$. Once again, the initial stages of drop spreading do not depend on the value of α, and they quantitatively agree with the spreading observed on a smooth, perfectly wetting glass substrate.[15]

Our experiments confirm that the final stages reached by a drop spreading on chemically striped substrates strongly depend on the value of α.[34,35] However, the initial dynamics along the parallel and perpendicular direction is not influenced by the presence of the chemical stripes. This initial isotropy was already shown for viscous drop spreading,[52] for which the initial dynamics is much slower. For water, the dynamics is dominated

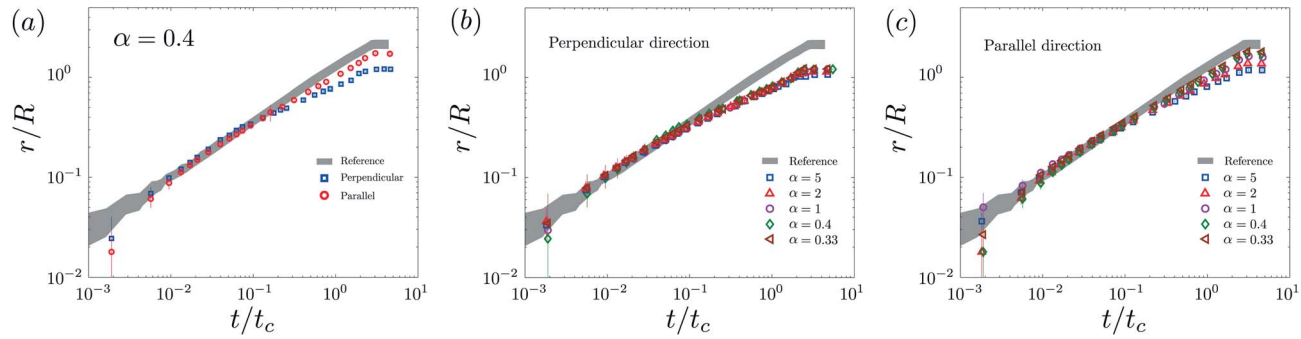

Fig. 4 (a) Dimensionless radius r/R as a function of dimensionless time t/t_c for a chemically striped structure with $\alpha = 0.4$. (b) Dimensionless radius r/R as a function of dimensionless time t/t_c along the perpendicular direction for 5 different values of α. (c) Dimensionless radius r/R as a function of dimensionless time t/t_c along the parallel direction for 5 different values of α.

by inertia. Both for the parallel and perpendicular directions, the initial spreading follows the 1/2 power-law, and within experimental error this dynamic behaviour is identical to that of perfectly wetting smooth silica.

3.3 Soft substrates

We finally investigate the spreading on soft substrates where both the elastic modulus G' and the sample thickness h can be varied. Very soft substrates are known to present a viscous braking-effect,[46,47] which might slow down the spreading of a water drop. Fig. 5(a) presents the growth of the dimensionless radius r/R as a function of the dimensionless time t/t_c for $G' =$ 32 kPa and four different sample thicknesses. We first observe that there is no effect of the sample thickness, as the spreading curve is the same for all values of h from 33 to 200 μm, in agreement with previous findings.[14] These substrates are highly hydrophobic ($\theta_{adv} = 135 \pm 5°$), leading to a small final radius $r_{eq}/R \simeq 0.6$. As a consequence, we do not observe an extended 1/2 power-law regime even if the initial regime agrees quantitatively with the reference curve provided by hard and smooth perfectly wetting glass substrates.[15]

This is further confirmed for substrates with a larger modulus $G' = 1.1$ MPa [Fig. 5(b)]. We observe the same qualitative behaviour, with an initial regime consistent with the 1/2 power law and a final state independent of the substrate thickness, with a slightly lower equilibrium contact angle ($\theta_{adv} = 120 \pm 5°$) and thus a slightly larger equilibrium radius $r_{eq}/R \simeq 0.7$. Finally, we can turn these soft substrates perfectly wetting by plasma cleaning them for 1 minute. Plasma cleaning alters the surface chemistry of the originally hydrophobic PDMS surface, leading to an SiOH terminated surface, which is hydrophilic with very small contact angles.[53] The results for the substrates with $G' = 32$ kPa are presented in Fig. 5(c). In this case, the spreading agrees quantitatively with that observed on hard and perfectly wetting substrates – despite the very low elastic modulus of the substrate.

From this we conclude that neither the elastic modulus G' nor the sample thickness h has any influence on the spreading behaviour. For perfectly wetting soft samples, the spreading follows the inertial 1/2 power law. For partially wetting substrates, the initial part of the spreading law agrees with this law but it deviates early to reach the equilibrium contact angle on the substrate.

4 Universality of spreading

From our experimental results we can deduce two main features of drop spreading on a complex substrate. First, the various

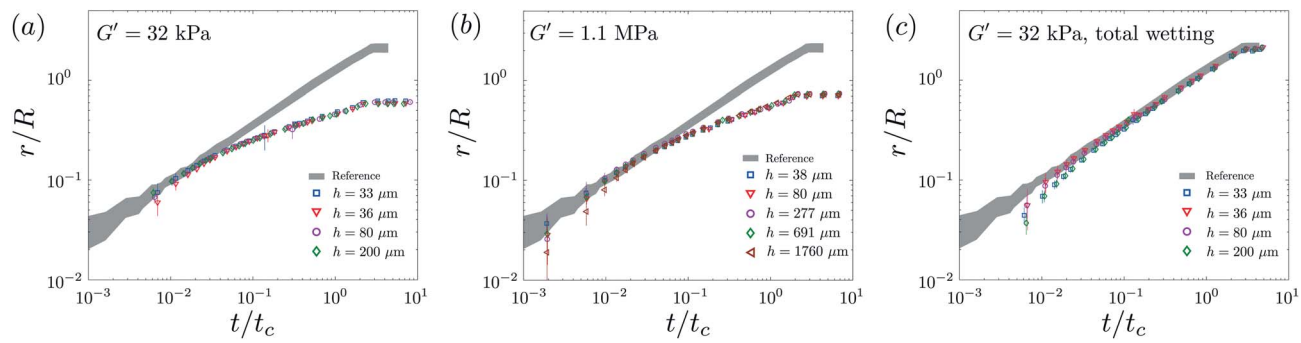

Fig. 5 (a) Dimensionless radius r/R as a function of dimensionless time t/t_c for a soft substrate with $G' = 32$ kPa under partially wetting conditions for 4 different sample thicknesses. (b) Dimensionless radius r/R as a function of dimensionless time t/t_c for a soft substrate with $G' = 32$ kPa under partially wetting conditions for 5 different sample thicknesses. (c) Dimensionless radius r/R as a function of dimensionless time r/t_c for a soft substrate with $G' = 32$ kPa under perfectly wetting conditions for 4 different sample thicknesses.

types of surface complexity do not affect the spreading during the initial stages: one recovers the same 1/2 power law, eqn (1), observed for smooth, rigid substrates.[10,11,15] When the complex substrates are perfectly wetting, this power-law is observed over several decades in time. The case of partially wetting substrates is more complex, as the wetted area cannot grow continuously: the spreading has to stop when the contact angle reaches θ_{adv}, the advancing equilibrium contact angle.

It is interesting to investigate the time at which the experimental data start to deviate from the 1/2 power-law, and to determine the cross-over behavior towards the final stage. We therefore measure the (dimensional) time τ where the measured radius r/R falls below 75% of the predicted value by eqn (1). We determine this "cross-over time" τ for each of the partially wetting experiments. The values of τ are plotted in Fig. 6(a) as a function of the advancing angle θ_{adv}. Intriguingly, there is a very convincing correlation between this cross-over time and the contact angle, despite the large variety of the substrates; the plot includes data from smooth partially wetting surfaces, chemically striped surfaces with different α and soft substrates. This strongly suggests that not only the initial dynamics is insensitive to the details of the substrate, but even the cross-over dynamics: it appears to be mainly determined by the final contact angle. In Fig. 6(b), we also plot the dimensionless spreading radius at the time τ, denoted by r_τ/R, as a function of the final radius after reaching equilibrium r_f/R. We find a good correlation that confirms that the deviation radius (and thus the deviation time) are set by the final contact angle θ_{adv}.

It is now tempting to evaluate whether there is a universal dynamics in the cross-over regime. If the dynamics is indeed governed by the cross-over time τ, we can attempt a following empirical law

$$\frac{r}{R} = \left(\frac{t}{t_c}\right)^{1/2} \mathscr{F}\left(\frac{t}{\tau}\right). \quad (2)$$

Here, the function $\mathscr{F}(t/\tau)$ describes the time-dependence of the spreading in the later stages, capturing the cross-over dynamics away from the very early regime. Hence, we postulate that that deviation from the 1/2 power-law is universal and expressed by a function $\mathscr{F}$ that depends only on the cross-over time τ, for all substrates. Clearly, one must find that $\mathscr{F}(0) = A = 1.2 \pm 0.1$, to recover the initial dynamics. To verify this hypothesis we rewrite (2) as

$$\frac{r}{R}\left(\frac{t_c}{\tau}\right)^{1/2} = \left(\frac{t}{\tau}\right)^{1/2} \mathscr{F}\left(\frac{t}{\tau}\right). \quad (3)$$

and try to collapse all data by plotting the left hand side as a function of t/τ. The result is shown in Fig. 6(c). Indeed, all experimental curves nicely collapse, confirming that even the cross-over appears to be universal for all substrates, and governed only by the final contact angle.

5 Conclusions

The initial spreading of low-viscosity drops on a smooth, perfectly wetting substrate exhibits a well-defined power-law dynamics $r \sim t^{1/2}$ over several decades. In this case, the spreading was previously found to be identical to that of the dynamics of coalescence of two low-viscosity, freely suspended, spherical drops, and the scaling law can be obtained by balancing capillary effects with liquid inertia.[10,11,15] Here, we have shown that this inertial regime also appears for complex substrates, namely micro-textured substrates, chemically striped substrates and soft substrates. Under perfectly wetting conditions, the power-law dynamics still extends over several decades, regardless of the complexity of the substrates, whereas one observes a deviation for partially wetting surfaces as the drop reaches a finite equilibrium contact radius.

For partially wetting surfaces, the departure from the inertial 1/2 power law appears to be universal and does not depend on the substrate complexity. The deviation time is set by the final contact angle, or equivalently the deviation radius is determined by the final contact radius of the drop. The collapse in Fig. 6(c) shows that partially wetting surfaces exhibit continuous crossover from a 1/2 power law, slowing down in order to match the final equilibrium radius r_f. This cross-over dynamics is in contrast with previous interpretations of the spreading on partially wetting substrates, for which the data were fitted by pure power-laws, $r \sim t^\beta$, with an exponent β that is a function of θ.[11,18] The collapse in Fig. 6(c) includes both extremely rigid glass substrates and PDMS of varying elasticity. Hence, we do not seem to observe any visco-elastic effects, as also suggested

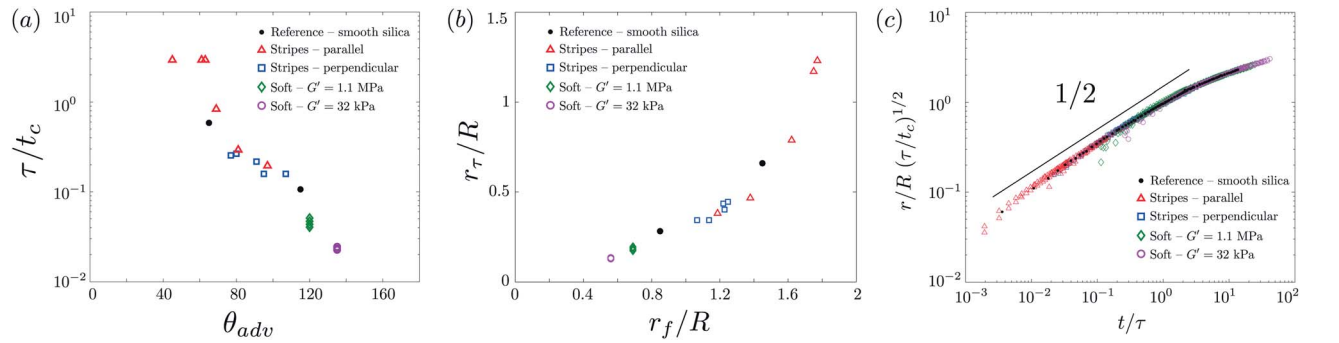

Fig. 6 (a) Dimensionless deviation time τ/t_c as a function of the final advancing contact angle θ_{adv} for all partially wetting substrates, including data from ref. 15. (b) Dimensionless deviation radius r_τ/R as a function of the dimensionless final radius r_f/R for the same dataset. (c) $r/R(\tau/t_c)^{1/2}$ as a function of t/τ for all partially wetting substrates, testing the proposed dynamics (3). The collapse reveals the universality of the cross-over.

by Fig. 5(c). This may be explained by the rapid contact line motion, probing relatively high frequencies for which G' is effectively higher. Namely, the simplest frequency that can be constructed is $f \sim \dot{r}/r$,[48] which owing to the power-law dynamics scales as $f \sim 1/t$. This means that during the course of our experiment, the frequencies of the material are probed roughly from MHz to kHz. In the rheometry, we were able to probe the substrates only up to 100 Hz, where we saw, similarly to previous results,[18] a dramatic increase of the stiffness (more than two orders of magnitude from 1 Hz to 100 Hz). This means that even extremely soft materials are very rigid during the course of the spreading experiment. Another estimate of the frequency would be $f \sim \dot{r}/d$, where d is the thickness of the sample. However, we found no thickness dependence of our results so we believe this is not a correct estimate. From all this, we conclude that the soft substrates are rigid on the time scale explored by the experiment, explaining why there is no viscous braking here.

The key open question is why the early stages of spreading are completely independent of the substrate properties. This can be explained from the singular geometry near the contact point, as shown in Fig. 7. Just after the contact, the meniscus connecting the drop and the substrate is extremely small, as it scales like $w \sim r^2/R$. This means that even when the wetted area has reached about 50 microns, the meniscus size w is only about 2 microns (Fig. 7). This induces a very strong curvature, and hence very large Laplace pressure difference inside the drop. Note that the pressure has to be lower close to the contact line, so that the flow is oriented from the bulk of the drop to the surface. This pressure jump is easily able to drive the liquid over substrate topography or chemical stripes. This strong Laplace pressure rationalizes that we see no influence of the spatial structures of the substrate, as long as w is small with respect to the substrate scales. This view is further supported by the quantitative agreement between drop spreading and drop coalescence:[24,25] when replacing the substrate by another droplet, for which the geometry of the meniscus is essentially the same as in Fig. 7, the observed dynamics is strictly identical. All this suggests that the initial motion $r(t)$ is not governed by the contact line, but rather by the transport of liquid from the center of the drop into the wetted region. Clearly, a more detailed analysis of the flow field inside the spreading drop is necessary to resolve this issue.

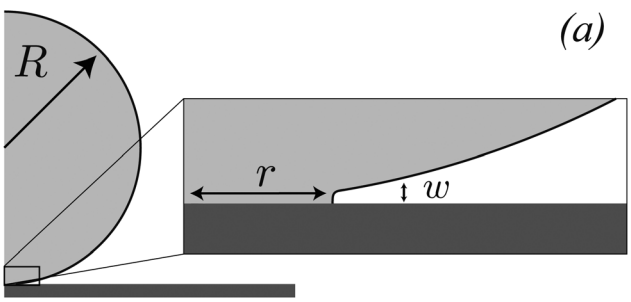

Fig. 7 Schematics presenting the geometry of a drop with an initial radius R during the initial stages of spreading. The width of the narrow gap w determines the local curvature and thus the driving force. It scales as $w \sim r^2/R$.

Acknowledgements

We would like to thank P.A. Tsai for providing micro-textured substrates as well as for fruitful discussion. We acknowledge E. Bonaccurso, L. Chen and M. Lopes for stimulating discussion as well as for sharing their experimental protocol for soft substrates. We thank K. G. Winkels for his help in designing the experimental set-up. This work was funded by VIDI Grant no. 11304.

References

1 H. Wijshoff, *Phys. Rep.*, 2010, **491**, 77–177.
2 P. Simpkins and V. Kuck, *J. Colloid Interface Sci.*, 2003, **263**, 562–571.
3 D. Bonn, J. Eggers, J. Indekeu, J. Meunier and E. Rolley, *Rev. Mod. Phys.*, 2009, **81**, 739–805.
4 V. Bergeron, D. Bonn, J. Y. Martin and L. Vovelle, *Nature*, 2000, **405**, 772–775.
5 P. G. De Gennes, *Rev. Mod. Phys.*, 1985, **57**, 827–863.
6 J. H. Snoeijer and B. Andreotti, *Annu. Rev. Fluid Mech.*, 2013, **45**, 269–292.
7 T. Young, *Philos. Trans. R. Soc. London*, 1805, **95**, 65–87.
8 P. G. de Gennes, F. Brochard-Wyart and D. Quere, *Capillarity and Wetting Phenomena: Drops, Bubbles, Pearls, Waves,* Springer, New York, 2003.
9 L. Tanner, *J. Phys. D: Appl. Phys.*, 1979, **12**, 1–14.
10 A.-L. Biance, C. Clanet and D. Quéré, *Phys. Rev. E: Stat., Nonlinear, Soft Matter Phys.*, 2004, **69**, 016301.
11 J. C. Bird, S. Mandre and H. A. Stone, *Phys. Rev. Lett.*, 2008, **100**, 234501.
12 L. Courbin, J. C. Bird, M. Reyssat and H. A. Stone, *J. Phys.: Condens. Matter*, 2009, **21**, 464127.
13 A. Carlson, M. Do-Quang and G. Amberg, *J. Fluid Mech.*, 2011, **682**, 213–240.
14 L. Q. Chen, G. K. Auernhammer and E. Bonaccurso, *Soft Matter*, 2011, **7**, 9084.
15 K. G. Winkels, J. H. Weijs, A. Eddi and J. H. Snoeijer, *Phys. Rev. E: Stat., Nonlinear, Soft Matter Phys.*, 2012, **85**, 055301.
16 A. Carlson, G. Bellani and G. Amberg, *Phys. Rev. E: Stat., Nonlinear, Soft Matter Phys.*, 2012, **85**, 045302.
17 A. Eddi, K. Winkels and J. Snoeijer, *Phys. Fluids*, 2013, **25**, 013102.
18 L. Q. Chen, E. Bonaccurso and M. E. R. Shanahan, *Langmuir*, 2013, **29**, 1893.
19 J. Eggers, J. R. Lister and H. A. Stone, *J. Fluid Mech.*, 1999, **401**, 293–310.
20 L. Duchemin, J. Eggers and C. Josserand, *J. Fluid Mech.*, 2003, **487**, 167–178.
21 M. Wu, T. Cubaud and C.-M. Ho, *Phys. Fluids*, 2004, **16**, L51–L54.
22 D. G. A. L. Aarts, H. N. W. Lekkerkerker, H. Guo, G. H. Wegdam and D. Bonn, *Phys. Rev. Lett.*, 2005, **95**, 164503.
23 J. D. Paulsen, J. C. Burton and S. R. Nagel, *Phys. Rev. Lett.*, 2011, **106**, 114501.

24 J. D. Paulsen, J. C. Burton, S. R. Nagel, S. Appathurai, M. T. Harris and O. A. Basaran, *Proc. Natl. Acad. Sci. U. S. A.*, 2012, **109**, 6857–6861.
25 A. Eddi, K. G. Winkels and J. H. Snoeijer, *Phys. Rev. Lett.*, 2013, **111**, 144502.
26 R. N. Wenzel, *Ind. Eng. Chem.*, 1936, **28**, 988–994.
27 A. B. D. Cassie and S. Baxter, *Trans. Faraday Soc.*, 1944, **40**, 546–551.
28 D. Quere, *Nat. Mater.*, 2002, 14–15.
29 M. Sbragaglia, A. M. Peters, C. Pirat, B. M. Borkent, R. G. H. Lammertink, M. Wessling and D. Lohse, *Phys. Rev. Lett.*, 2007, **99**, 156001.
30 C. Pirat, M. Sbragaglia, A. Peters, B. Borkent, R. Lammertink, M. Wessling and D. Lohse, *Europhys. Lett.*, 2008, **81**, 66002.
31 P. Tsai, R. van der Veen, M. van de Raa and D. Lohse, *Langmuir*, 2010, **26**, 16090.
32 P. Tsai, M. Hendrix, R. Dijkstra, L. Shui and D. Lohse, *Soft Matter*, 2011, **7**, 11325.
33 J. Y. Chung, J. P. Youngblood and C. M. Stafford, *Soft Matter*, 2007, **3**, 1163–1169.
34 O. Bliznyuk, E. Vereshchagina, E. S. Kooij and B. Poelsema, *Phys. Rev. E: Stat., Nonlinear, Soft Matter Phys.*, 2009, **79**, 041601.
35 E. S. Kooij, H. P. Jansen, O. Bliznyuk, B. Poelsema and H. J. W. Zandvliet, *Colloids Surf., A*, 2012, **413**, 328–333.
36 O. Bliznyuk, H. P. Jansen, E. S. Kooij, H. J. W. Zandvliet and B. Poelsema, *Langmuir*, 2011, **27**, 11238–11245.
37 H. P. Jansen, K. Sotthewes, C. Ganser, C. Teichert, H. J. W. Zandvliet and E. S. Kooij, *Langmuir*, 2012, **28**, 13137–13142.
38 R. Pericet-Camara, A. Best, H.-J. Butt and E. Bonaccurso, *Langmuir*, 2008, **24**, 10565–10568.
39 R. W. Style and E. R. Dufresne, *Soft Matter*, 2012, **8**, 7177–7184.
40 A. Marchand, S. Das, J. H. Snoeijer and B. Andreotti, *Phys. Rev. Lett.*, 2012, **109**, 236101.
41 A. Marchand, S. Das, J. H. Snoeijer and B. Andreotti, *Phys. Rev. Lett.*, 2012, **108**, 094301.
42 L. Limat, *Eur. Phys. J. E*, 2012, **35**, 134.
43 J. Weijs, B. Andreotti and J. Snoeijer, *Soft Matter*, 2013, **9**, 8494.
44 R. W. Style, R. Boltyanskiy, Y. Che, J. S. Wettlaufer, L. A. Wilen and E. R. Dufresne, *Phys. Rev. Lett.*, 2013, **110**, 066103.
45 R. W. Style, Y. Che, S. J. Park, B. M. Weon, J. H. Je, C. Hyland, G. K. German, M. P. Power, L. A. Wilen, J. S. Wettlaufer and E. R. Dufresne, *Proc. Natl. Acad. Sci. U. S. A.*, 2013, **110**, 12541–12544.
46 M. E. R. Shanahan and A. Carré, *Langmuir*, 1995, **11**, 1396–1402.
47 A. Carré, J.-C. Gastel and M. E. R. Shanahan, *Nature*, 1996, **379**, 432–434.
48 T. Kajiya, A. Daerr, T. Narita, L. Royon, F. Lequeux and L. Limat, *Soft Matter*, 2013, **9**, 454–461.
49 M. C. Lopes and E. Bonaccurso, *Soft Matter*, 2012, **8**, 3875.
50 C. Extrand and Y. Kumagai, *J. Colloid Interface Sci.*, 1996, **184**, 191–200.
51 D. Long, A. Ajdari and L. Leibler, *Langmuir*, 1996, **12**, 5221.
52 O. Bliznyuk, H. P. Jansen, E. S. Kooij and B. Poelsema, *Langmuir*, 2010, **26**, 6328–6334.
53 J. C. McDonald, D. C. Duffy, J. R. Anderson, D. T. Chiu, H. Wy, O. J. A. Schueller and G. M. Whitesides, *Electrophoresis*, 2000, **21**, 27–40.